NEUROSCIENCE

Dopamine and beta-band oscillations differentially link to striatal value and motor control

H. N. Schwerdt[1,2]*, K. Amemori[1]†, D. J. Gibson[1], L. L. Stanwicks[1], T. Yoshida[1], N. P. Bichot[1], S. Amemori[1]†, R. Desimone[1], R. Langer[2,3], M. J. Cima[2,4]*, A. M. Graybiel[1]*

Parkinson's disease is characterized by decreased dopamine and increased beta-band oscillatory activity accompanying debilitating motor and mood impairments. Coordinate dopamine-beta opposition is considered a normative rule for basal ganglia function. We report a breakdown of this rule. We developed multimodal systems allowing the first simultaneous, chronic recordings of dopamine release and beta-band activity in the striatum of nonhuman primates during behavioral performance. Dopamine and beta signals were anticorrelated over seconds-long time frames, in agreement with the posited rule, but at finer time scales, we identified conditions in which these signals were modulated with the same polarity. These measurements demonstrated that task-elicited beta suppressions preceded dopamine peaks and that relative dopamine-beta timing and polarity depended on reward value, performance history, movement, and striatal domain. These findings establish a new view of coordinate dopamine and beta signaling operations, critical to guide novel strategies for diagnosing and treating Parkinson's disease and related neurodegenerative disorders.

INTRODUCTION

In Parkinson's disease, a progressive loss of dopamine occurs in the striatum, a key input-output hub of the basal ganglia (*1*). Beta-band oscillatory activity, indicative of synchronization of neural activity, increases in the basal ganglia as dopamine levels decline. Dopamine replacement therapy, used in treating patients with Parkinson's disease, is associated with a reduction in beta-band oscillations (*2*). Clinical trials are underway to use beta-band monitoring in these patients as an inverse proxy for dopamine levels (*2–4*) in open- and closed-loop deep brain stimulation (DBS) (*5*, *6*). However, the diagnostic power of these beta signals and their relationship to dysregulated dopamine levels remain unresolved (*7–10*). Simultaneous monitoring of dopamine (chemical) and beta (electrical) activities is necessary to test their relationships, but such measurements have not yet been possible in primates including humans, due to formidable technical problems (*11*). We now have developed a multimodal platform allowing such simultaneous measurements by combining fast-scan cyclic voltammetry (FSCV) to measure dopamine release and electrical recording from arrays of miniature probes chronically implanted in the macaque striatum (figs. S1 and S2 and table S1). We asked whether dopamine levels and beta-band oscillatory local field potential (LFP) activity (fig. S3) are strictly inverse in the context of processing reward value and motor performance and whether their relationships vary as a function of the sites recorded from in the striatum. We recorded dopamine release and beta-band LFPs in rhesus monkeys performing tasks in which they needed to make saccadic eye movements to a left or right target displayed on a screen in front of them to receive small or large amounts of food reward. These recordings yielded measures of reward value and movement control (*11*, *12*), aspects of which are known to be associated with dopamine and beta-band oscillations and are compromised in Parkinson's disease. Trial-by-trial measures of dopamine and beta-band LFPs allowed a side-by-side comparison of these two signaling modalities during the same time frames and behavioral events.

RESULTS

Monitoring and classifying task-modulated features of dopamine and beta-band activity

We developed multimodal systems to measure concurrently both electrical and chemical neural activity and to test directly the relationship between dopamine levels and beta-band activity with sub-second temporal resolution at the microscale level (Fig. 1, A and B). Signals were recorded from the caudate nucleus (CN) and putamen over 3 to 6 months as monkeys performed the visually guided tasks for reward (RW) (Fig. 1C). Concurrent measurements of electrical and chemical neural activity were made in monkey 1 (M1), and only chemical signals were recorded in M2. A trial began with the display of a central cue to which the monkey had to saccade and fixate. Then, this central cue disappeared, and a peripheral target was displayed, in random sequence, on the left (contralateral to recording sites) or on the right (ipsilateral) side of the screen. The monkey then had to saccade to and fixate on this peripheral target for 4 s to successfully complete a trial and receive a large or small RW. The size of RW (large or small) depended on the target side (contralateral or ipsilateral to the recordings), and the side associated with either RW size switched after a block of 15 to 45 trials. We focused our analyses on the 4-s period between target onset (T) and RW (the T-RW period), during which expectation of RW (large and small) and motor control features could be defined. We estimated the animals' internal states during the T-RW period by recording lick rate, pupil diameter, reaction time, and heart rate. All of these physiological parameters were different for the large and small RW tasks (Fig. 1D).

[1]McGovern Institute for Brain Research and Department of Brain and Cognitive Sciences, Massachusetts Institute of Technology, 43 Vassar Street, Cambridge, MA 02139, USA. [2]Koch Institute for Integrative Cancer Research, Massachusetts Institute of Technology, Cambridge, MA 02139, USA. [3]Department of Chemical Engineering, Massachusetts Institute of Technology, Cambridge, MA 02139, USA. [4]Department of Materials Science and Engineering, Massachusetts Institute of Technology, Cambridge, MA 02139, USA.
*Corresponding author. Email: schwerdt@mit.edu (H.N.S.); mjcima@mit.edu (M.J.C.); graybiel@mit.edu (A.M.G.)
†Present address: The Hakubi Center for Advanced Research and Primate Research Institute, Kyoto University, 41-2 Kanrin, Inuyama, Aichi 484-8506, Japan.
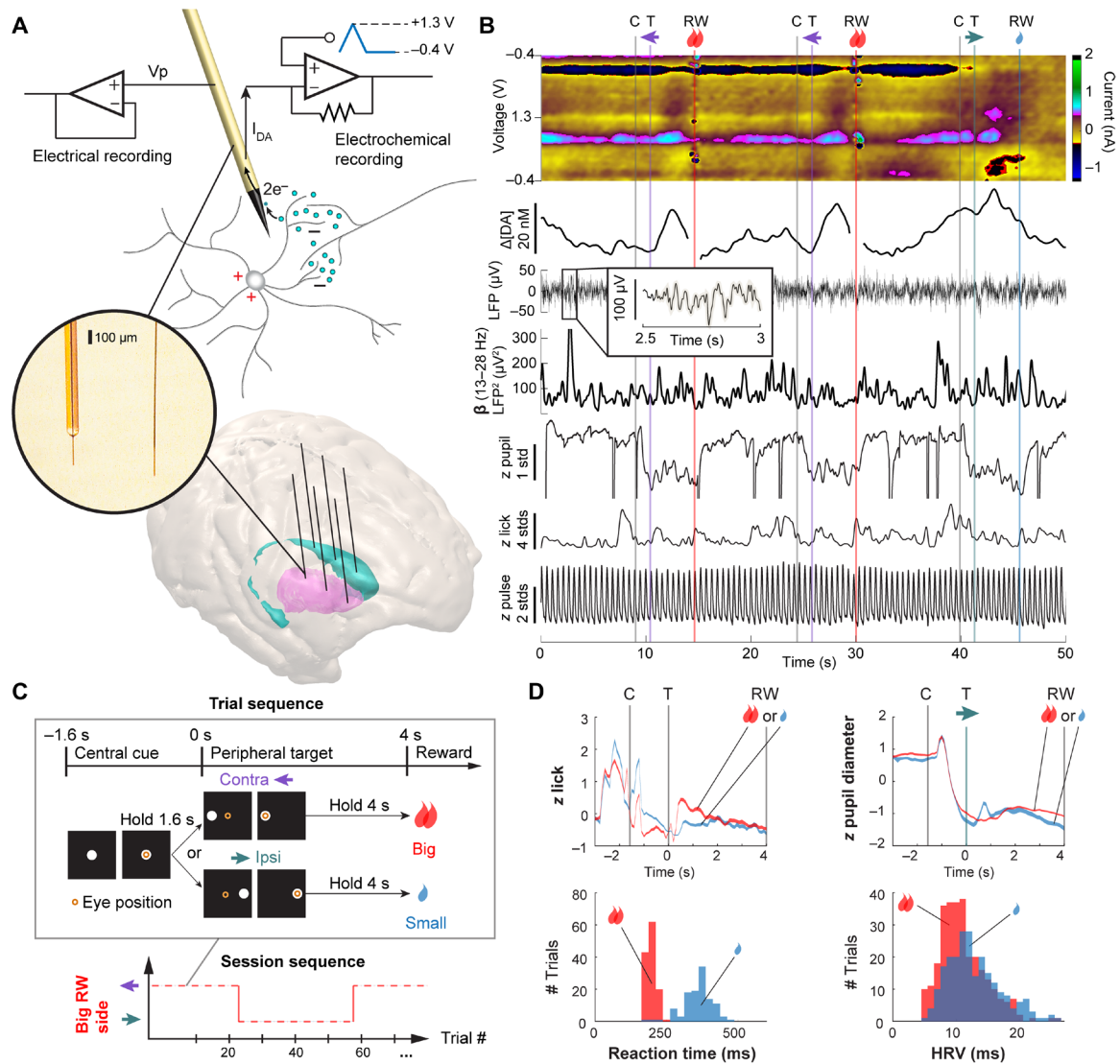
Fig. 1. Systems for multimodal recording of physiological activity in behaving primates. (**A**) Setup for recording electrical activity (left) and dopamine activity (right) from an implanted moveable silica probe (inset photo left) or fixed microinvasive probe (photo right) in the striatum. (**B**) Example of synchronous recording of dopamine (Δ[DA]), LFP, filtered beta-band (β) LFP power, pupil diameter, lick activity, and pulse during task performance recorded from M1. C, central cue onset; T, peripheral target onset; RW, reward onset. (**C**) Visually guided reward-biased task. In the block shown, the contralateral (Contra) target was associated with a big RW. Contralateral and ipsilateral (Ipsi) target trials were introduced randomly in sequence within a block, and the target side associated with a big RW switched between blocks (15 to 45 trials). (**D**) Physiological responses and reaction time from M1, aggregated over groups of big and small RW trials, demonstrating discrimination of RW size in a single session. Trace thickness is equal to ±SE.

Task-modulated dopamine and beta-band signals measured with the same time windows and sampling rates occurred at very different time scales. Dopamine displayed prolonged increases or decreases, reaching peak values over a wide distribution of time points ranging the entire T-RW period from 0.2 to 3.8 s following target onset (mean range of 2.1 to 3 s) (Fig. 2, A and B, right). These peak values were found to distinguish task conditions more accurately than averages over the T-RW periods (Figs. 3 to 5 and figs. S4 and S5). These prolonged dynamics were similar to those reported for dopamine ramping signals (*13*) and the adaptive firing rates of dopamine neurons (*14*). By contrast, beta-band activity displayed an immediate suppression or "event-related desynchronization" (ERD) (*2*) during the period from 0.35 to 0.6 s after target onset (Fig. 2, A and B, right) that defined a time period for task-related modulation of the beta signal earlier than that of the peak

dopamine signal. Windows applied sequentially across the entire T-RW period validated this early time period as one in which beta-band power (here designated as "early beta") significantly discriminated task conditions (large versus small RW trials and contralateral versus ipsilateral target trials) at the maximum number of sites (see the "Signals related to large and small reward" section in Materials and Methods). The same was true for validation of the dopamine peak metrics. Thus, we compared the time frames at which the dopamine and beta-band signals were maximally sensitive to task demands and conditions. The common pattern was that the decreases in early beta-band activity preceded, rather than followed, the peak dopamine responses. All measurements discussed below refer to these identified task-modulated posttarget dopamine peaks and early beta suppression metrics, as extracted over millisecond sampling periods, unless otherwise noted.
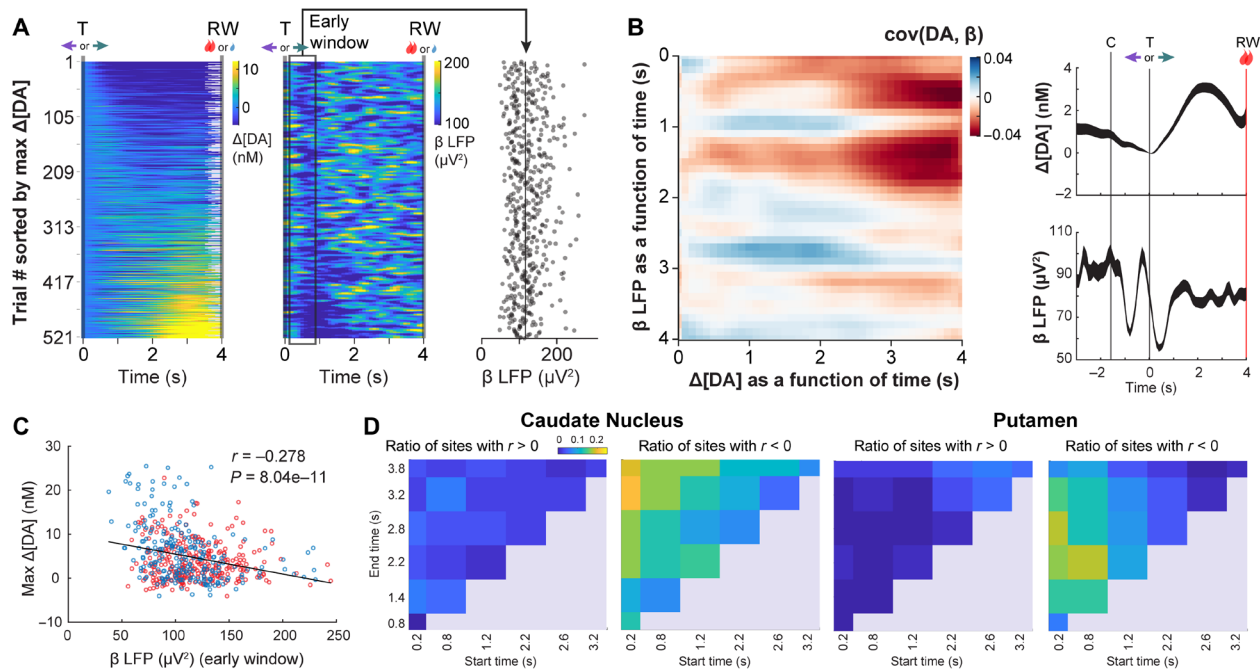
Fig. 2. Correlations between dopamine and beta-band signals as defined over short time scales. (**A**) T-aligned Δ[DA] (left) and β LFP (center) measured in the putamen across trials (rows) sorted for increasing peak Δ[DA] for an individual session with corresponding average early (0.2 to 0.8 s) β LFP (right, vertical line represents median value). (**B**) Covariance between dopamine and beta as a function of time relative to T for each of the two measurements, averaged across all sessions (left). Trial averaged time course of Δ[DA] (top) and β LFP (bottom) for big RW trials in a single session (right). Trace thickness is equal to ±SE. (**C**) Peak changes in dopamine (Δ[DA]) plotted versus early β LFP for the same site pair shown in (A), displaying significant anticorrelation (r and P values indicated in plot). (**D**) Matrices of the fraction of sites in the CN (left two plots) or putamen (right two plots), displaying significant positive (r > 0) or negative (r < 0) correlations between dopamine peaks and β LFP as computed by averaging over windows with different start (x axis) and end (y axis) times relative to T. Color indicates the ratio of sites displaying significant correlations, and a uniform scale is applied to all plots. All measurements are from M1.

Covariance calculations between dopamine and beta activity on average exhibited a weak anticorrelated dopamine-beta relationship that was strongest when the change in dopamine signals greatly lagged behind changes in beta signals (3.9 s versus 0.7 s relative to T; Fig. 2, B and C; see the "Beta-band power signal processing" section in Materials and Methods). These correlated time frames closely coincided with the task-modulated posttarget dopamine peak and early beta time frames. We examined the metrics of beta signaling outside of the identified task-modulated early beta time frame to look for correlations to dopamine across multiple time scales, examining all sessions, recording sites, and task conditions (table S2). These measurements included averaging beta power over a variety of windows of variable duration and times during the T-RW period (Fig. 2D), as well as computation of the ERD latency (15). Statistically significant anticorrelations occurred at 19% of all session-sites (Fig. 2D and table S2). Only a statistically insignificant number of positive correlations were found (<3% of all session-sites; average r = 0.108 for all session-sites with positive correlations; table S2). ERD latency produced negligible negative or positive correlations (<3%). The small magnitude of the observed anticorrelations (average r = −0.128, −0.139, or −0.126 for all sites, all CN session-sites, or all putamen session-sites, respectively, with negative correlations; see the "Correlational analyses" section in Materials and Methods), however, suggested that other factors might have influenced beta and dopamine levels, causing them to dissociate under certain conditions. We therefore examined recordings in relation to controlled task parameters such as movement requirements, and also those of esti-

mated internal states of motivation and arousal, including aspects of reward value and past history, alongside recorded physiological response signals to delineate such conditions.

Coactivity of dopamine and beta in specialized aspects of reward value

Measurements of signals recorded in the CN and putamen yielded contrasting patterns of dopamine-beta coactivity modulated by reward sensitivity and target position relative to recording hemisphere. The measured signals exhibited multiplexing of variables markedly affecting the polarities of dopamine and beta modulations during the T-RW period and whether those polarities were the same or opposite. Reward-sensitive dopamine and beta coactivity were examined by comparing neural responses grouped for large and small RW trials under fixed movement conditions (e.g., reward-biased responses for only contralateral target trials; Fig. 3A). Dopamine responses were selectively enhanced for contralateral targets compared to ipsilateral, and this preference was significant at 21% of sites (fig. S4A) (12, 16). Dopamine increases in the CN for large relative to small RW conditions (63% of all session-sites) were of opposite sign to the reductions in beta (50% of all session-sites; Fig. 3B and figs. S4 to S7), in keeping with expectations of a negative correlation between dopamine and beta. The situation was different for the putamen.

The expected inverse signaling patterns of dopamine and beta in response to these reward conditions were not found in the putamen (Fig. 3C). Instead, increases and decreases in dopamine responses occurred at discrete spatial locations in the putamen, whereas beta-band
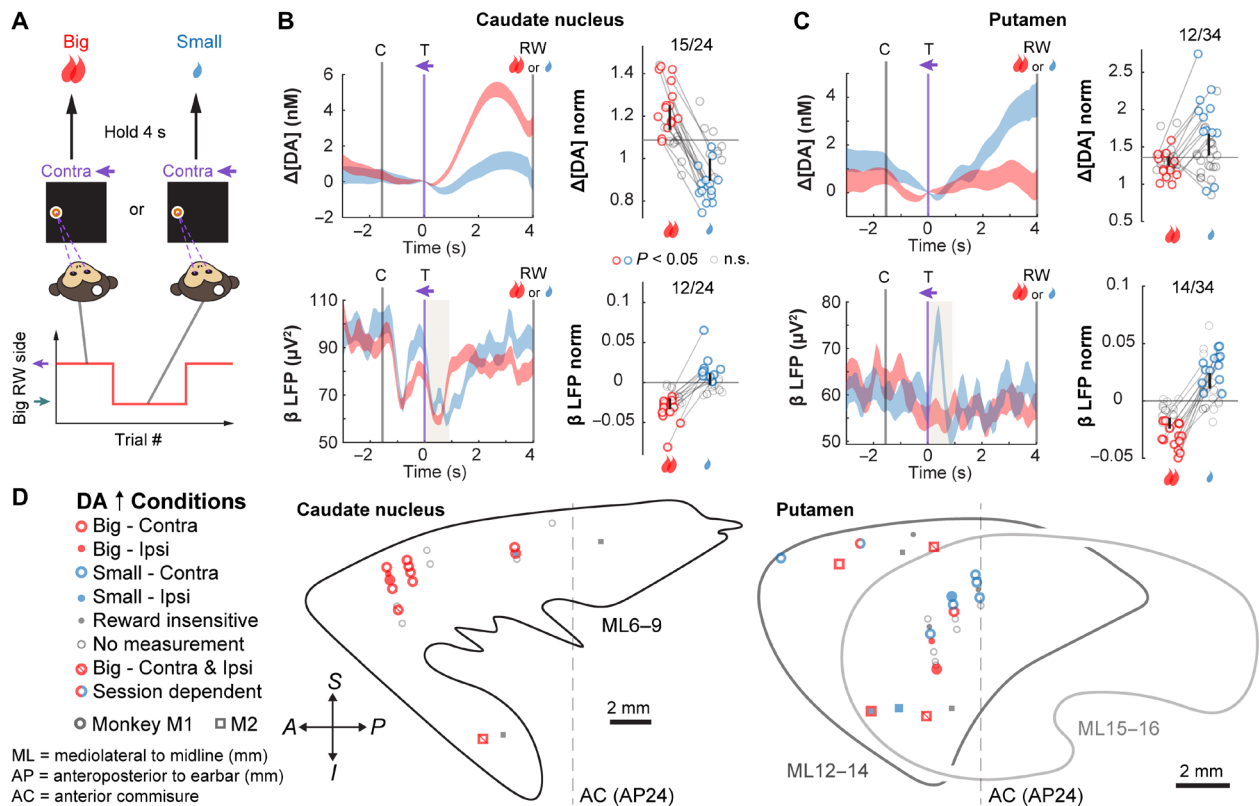
Fig. 3. Dopamine and beta selectivity to reward size inversely modulated in the CN but not putamen. (**A**) Illustration of trial procedure. The monkey holds its gaze on a contralateral target for 4 s to receive a big or small RW depending on the target side–RW size contingency for the given block of trials. (**B**) Δ[DA] (top left) and its paired β LFP (bottom left; early beta time window shaded) concurrently recorded from a single session in the CN, aligned to T (at 0 s). Line thickness is equal to ±SE. Scatter plots show normalized Δ[DA] peaks (top right) and paired early beta signals (bottom right) recorded concurrently for all sites in CN as averaged for each session (each circle) for contralateral movement conditions from M1. Δ[DA] and beta were normalized to the median or the minimum and maximum values, respectively (details in Materials and Methods). Lines are drawn between conditions for each site that showed a significant difference ($P < 0.05$, t test, colored circles), and the ratio of these sites is shown above the plot. Error bars indicate 95% confidence intervals. (**C**) Same as (B) but for putamen. (**D**) Sagittal views of dopamine-recorded sites in M1 (circles) and M2 (squares). Symbols denoted by color indicating specific RW condition and outline/fill pattern indicating specific movement condition, where Δ[DA] was significantly greater. AC, anterior commissure.

activity exhibited positive reward value signaling throughout the sites in the putamen that were sampled, as found in the CN (Fig. 3D and fig. S4B). Thus, dopamine release and beta activity were not universally anticorrelated. Moreover, the heterogeneity of our measured dopamine signals diverged from the predominant view of dopamine as a global reward signal (13, 17–19). Unexpectedly, in contrast to sites in the CN, the majority (83%) of reward-sensitive dopamine sites in the putamen preferred small RW for contralateral targets (Fig. 3C). Only two sites in the putamen exhibited higher dopamine levels for large versus small RW at the contralateral target, whereas preferences for large RW were more common at the ipsilateral target (fig. S4A). The sensitivities to reward size for the contralateral target were thus of the same polarity for dopamine and beta in putamen, in contrast to expectations of negative correlations for these two signaling modalities.

Disparity between effects of past history on dopamine and beta signals

We investigated the influence of past reward and performance experiences, which influence internal motivational states (20), on dopamine and beta signals. These were analyzed during fixed reward conditions, on the basis of whether the monkey had, on the previous trial, re-

ceived a large or small RW, or had made an error (Fig. 4A). These past experiences significantly modulated dopamine signals but not beta-band activity (Fig. 4, B and C, and figs. S5C and S6C).

Small rewards and performance failures consistently generated higher levels of dopamine on the subsequent trials. These effects of past history occurred for a large fraction of the dopamine signals recorded in both the CN (48%; Fig. 4B, top) and the putamen (35%; Fig. 4C, top). By contrast, only a handful of beta recordings in either the CN or the putamen were modulated, by either previous trial reward size or previous trial success [Fig. 4, B (bottom) and C (bottom), and figs. S5C (right) and S6C]. This lack of effect of prior events sharply contrasts with the recently uncovered role of beta in processing information about immediate reward (Fig. 3) (21). Thus, the dopamine and beta signals appear to subserve different, specialized aspects of motivation related to value and ongoing motivational levels integrating past events. These results corroborate the history sensitivity of dopamine signaling (20) and contradict the expectation of anticorrelation of the dopamine and early beta-band signals.

Coactivity of dopamine and beta in aspects of motor processing

We compared responses for saccades made to contralateral and ipsilateral targets for a fixed reward condition for dopamine and beta
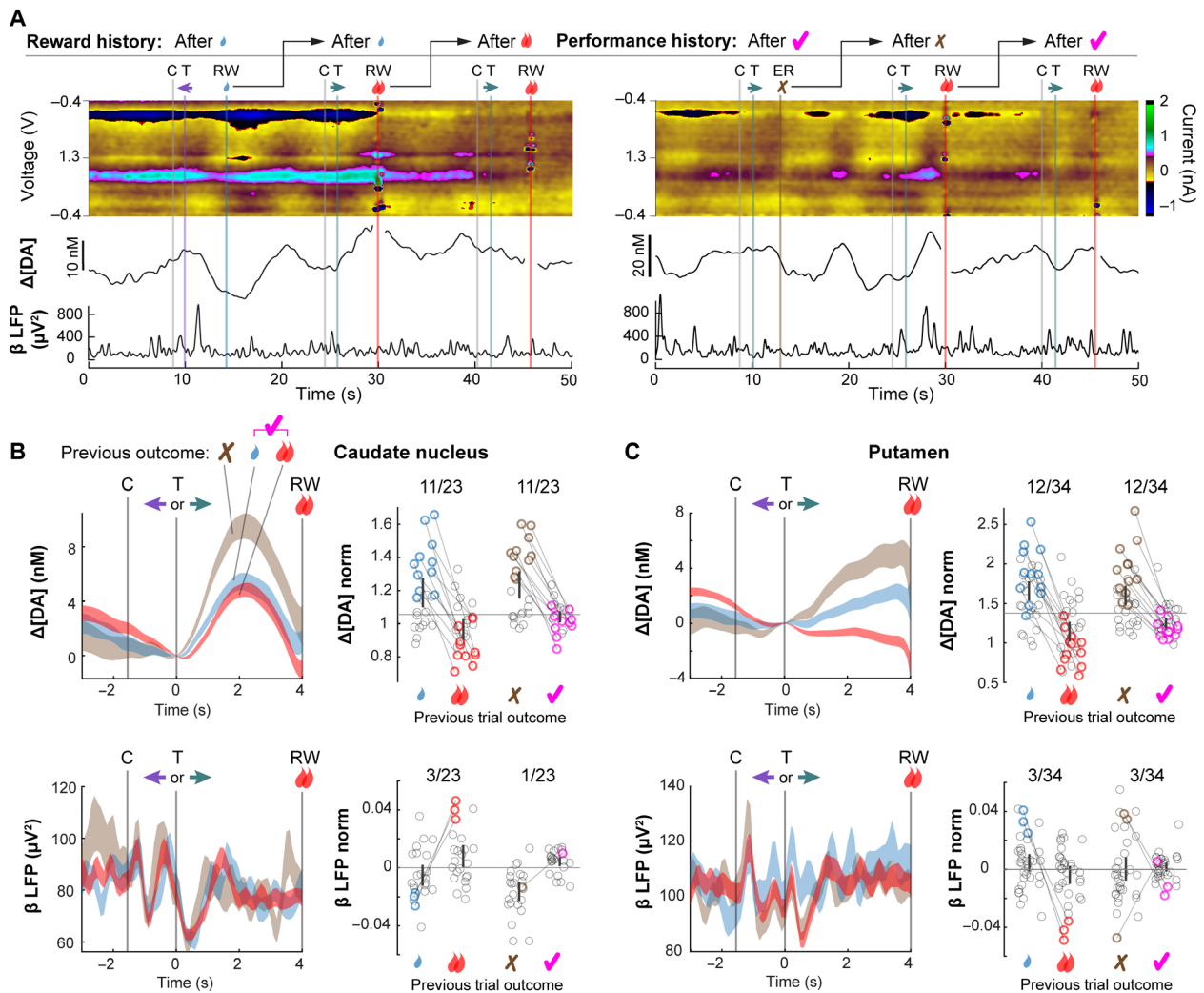
Fig. 4. Dopamine and beta signaling to reward and performance history. (**A**) (Left) Representative Δ[DA] and concurrently recorded β LFP from a paired site in the CN during a series of big and small RW trials. Δ[DA] increases immediately after T (26 to 30 s) when a small RW had been obtained on the previous trial, and decreases (42 to 46 s) when a big RW had been delivered on the previous trial. (Right) Same as left for measured Δ[DA] and β LFP over a sequence of failed and rewarded trials to demonstrate influence of performance history on recorded signals. Δ[DA] increases after T (26 to 30 s) when the animal failed to fixate on the target for a full 4 s on the preceding trial (failure) and increases to a smaller degree on the next trial (42 to 46 s) when it successfully completed the sequence of eye movements and received an RW on the previous trial. (**B**) (Left) Concurrently recorded Δ[DA] (top) and paired β LFP (bottom) on large reward trials, as shown in Fig. 3B, averaged for different outcomes on previous trial: failure (fixation break, brown), small RW (blue), and big RW (red) in CN. (Right) Scatter plot, as shown in Fig. 3B, for different outcome histories, for big RW trials. (**C**) Same as (B) but for putamen. All measurements are from M1.

(Fig. 5A). Opposite direction selectivity for dopamine and beta was found in many sites in the putamen (Fig. 5, C and D). Nearly all (92%) of the direction-sensitive dopamine responses in the putamen in small RW trials were larger for contraversive movements (Fig. 5C, top), in accord with lateralization of striatal function (*12*). These dopamine increases were inversely related to the suppressed responses of beta in the putamen (Fig. 5C, bottom). However, there was reduced dopamine release in the CN for contraversive movements relative to ipsiversive movements in small RW trials, whereas there was decreased beta-band activity also in the CN, as was observed in the putamen (Fig. 5B and fig. S4, F and G). This result once again frustrated expectations of opposite response polarities for beta-band activity and dopamine release, this time in the CN, but not in the putamen.

The direction selectivity of dopamine signals was split in large RW trials in both the CN and the putamen (Fig. 5D and figs. S4 to S7). Both dopamine and beta provided signals related to aspects of eye movement control, but dopamine displayed more heterogeneity in direction sensitivity that depended on reward context in some sites in both CN and putamen (Fig. 5D, note circles with opposite colors of fill and outline). By contrast, beta-band activity generated uniform patterns of suppressed signaling to contralateral cues in both striatal divisions for both large and small RW trials (fig. S6). Thus, an inverse pattern of dopamine and beta signaling was demonstrated in the context of motor control specifically in the putamen and was mostly associated with conditions (i.e., small RW) in which dopamine signals in the putamen had been found earlier to be more responsive (Fig. 3C). These movement-selective inverted signaling
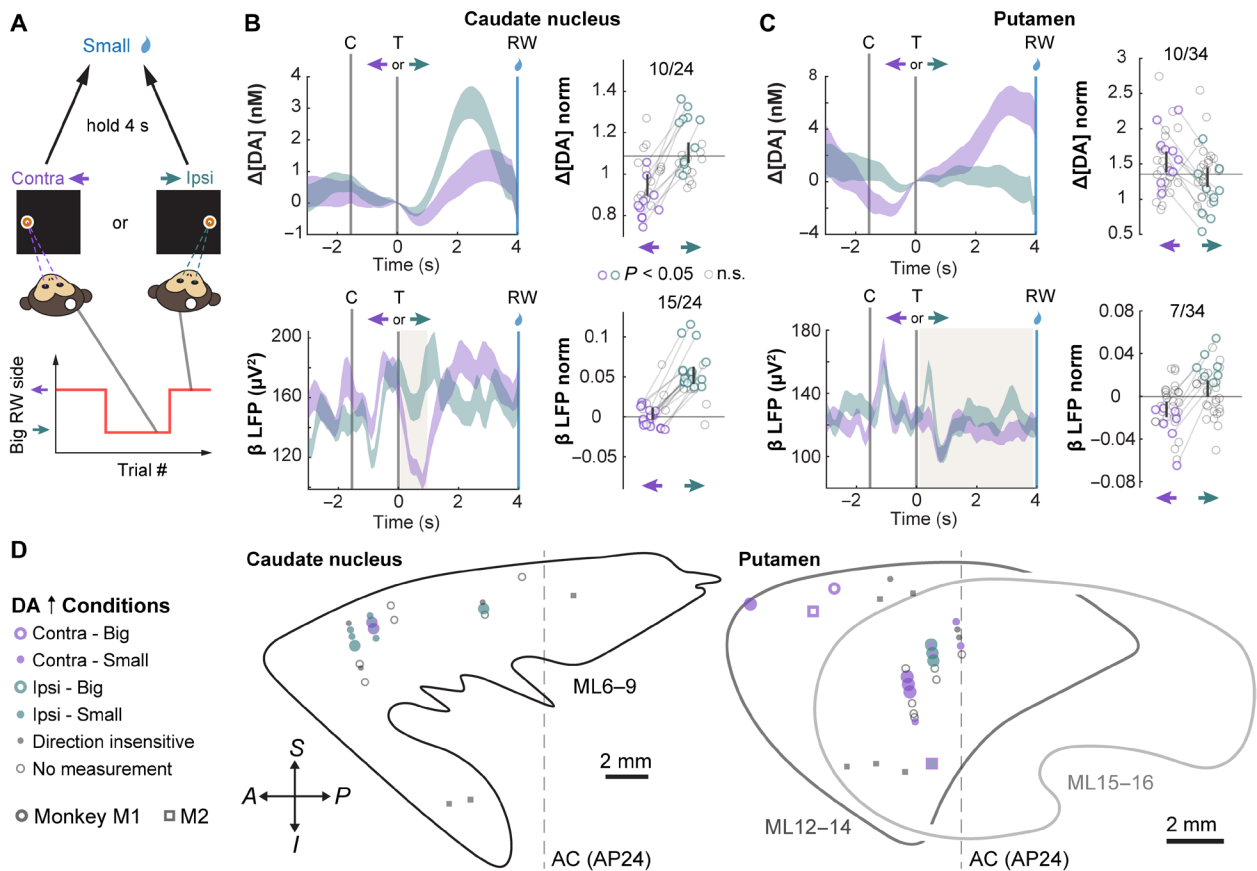
Fig. 5. Dopamine and beta signals associated with movement control. (**A**) Trial procedure in which the monkey fixated either a contralateral or ipsilateral target for 4 s to receive a small RW. (**B**) (Left) Representative measurements of Δ[DA] (top) and β LFP (bottom) in CN. (Right) Scatter plots of all measured sites in the CN from M1, comparing signals evoked by contralateral and ipsilateral targets for small RW as shown in Fig. 3B. (**C**) Same as (B) but for putamen. β LFP in the putamen best discriminated target positions when averaged over the entire target window (0.2 to 3.8 s, shaded). β LFP norm averaged over target window (right) for putamen sites only. (**D**) Spatial map of recorded responses as shown in Fig. 3D.

responses of the putamen contrasted with the same polarity patterns of dopamine and beta modulations observed in the CN, against the expected theory of anticorrelation.

The signals from sites that displayed significant responses to reward or movement task variables (Figs. 3, B and C, and 5, B and C) were selected to evaluate whether the consonance or dissonance in task sensitivities resulted in corresponding correlations between ongoing dopamine and beta activity sampled simultaneously in individual trials. Task modulation of dopamine and beta turned out to be remarkably independent of each other. The number of paired recordings that showed the task modulation of both dopamine and beta was not significantly different from the number expected by chance coincidence of independent dopamine modulation and beta modulation (binomial test, $P \geq 0.1$ for Figs. 3B and 5, B and C; $P = 0.054$ for Fig. 3C when both dopamine and beta preferred small RW in putamen in more than the expected number of site pairs). Therefore, the presence of dopamine modulation at a given site pair did not reflect either the absence or presence of beta modulation, and conversely, beta modulations were not reflected in the dopamine modulations. Furthermore, the number of these paired recordings that showed either positive or negative correlations was negligible (≤ 3 for any given task condition). Thus, the simultaneously measured signals did not conform to the view of anticorrelation even when they produced

inverse task-modulated responses. These results distinguish the independent time frames of dopamine and beta, as measured over a trial-by-trial basis, in signaling task-related reward value and movement parameters, from the synchronous dopamine-beta signaling time frames sampled over an individual trial. The collaborative function of the dopamine and beta signals in processing reward value and movement control may differ from the potential role afforded by their covarying activities (Fig. 2, B and D). We infer that factors for which we did not control in this analysis contributed strong enough negative correlations between beta and dopamine so that the positive correlation due to reward size was cancelled out. Physiological response signals synchronously recorded with the neural signals and outside of the fixed controlled task parameters were thus evaluated to further determine the degree to which other behavioral inputs provide a common input to dopamine and beta activity and the degree of their correlated activity.

Behavioral measures discriminate dopamine and beta activation in distinct aspects of motivation, arousal, and performance

Marked differences between the dopamine and early beta signals were apparent also when we analyzed their potential correlations with putative internal state measures (Fig. 6, A to E). The association between
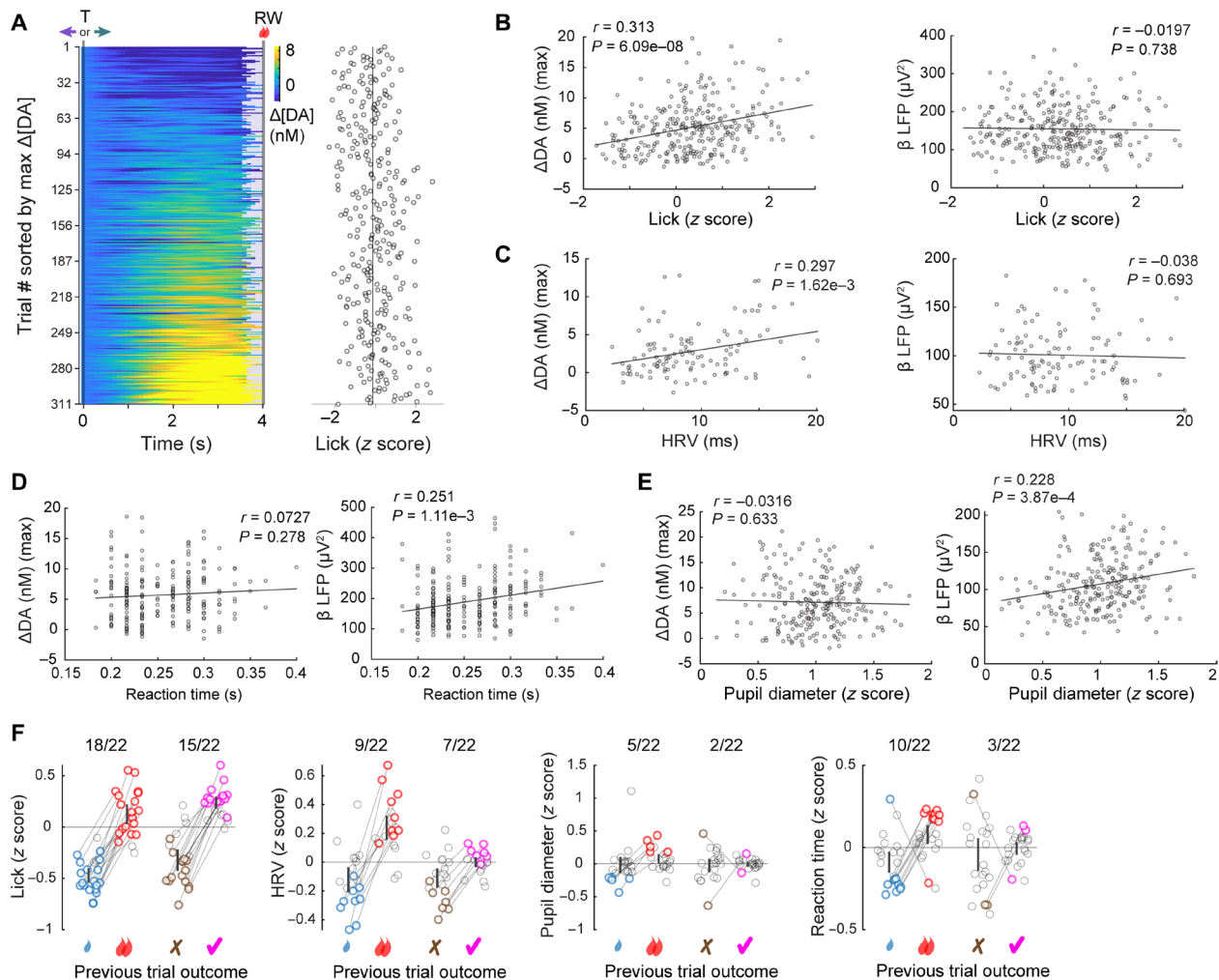
Fig. 6. Online measures of arousal, motivation, and motor performance related to dopamine and beta as well as past experiences (a task defined proxy of on-going motivational drive). (**A**) Trial-by-trial measures of dopamine as shown in Fig. 2A but for a different session, sorted by max Δ[DA] (left) with the corresponding z score of the licking activity (right). (**B**) Max Δ[DA] (left) and early beta (right) versus licking. Only dopamine shows a significant correlation to licking in this session. (**C** to **E**) Same as (B) for HRV (C), reaction time (D), and pupil diameter (E). (**F**) Scatter plot, as shown in Fig. 4B, of licking activity, HRV, pupil diameter, and reaction time for different outcome histories, measured for fixed big RW trial conditions. All measurements are from M1.

these measures and internal motivational states was also apparent in their high level of sensitivity to past experiences (Fig. 6F) (*21*). Anticipatory licking, related to incentive motivation and arousal, correlated positively with peak dopamine concentration changes in the CN (67% of all session-sites) and, to a lesser degree, correlated negatively with the early beta signals measured in the same trials (48% of all CN session-sites) (Fig. 6, A and B, and table S2). Heart rate variability (HRV), a proxy for parasympathetic drive and arousal, correlated positively with peak dopamine concentration changes in the CN (21%) and the putamen (15%), but only rarely with beta signals and only when averaged over broader windows (12%; table S2) measured in the same trials (Fig. 6C). The unique correlation between parasympathetic inputs to dopamine but not beta activity further opposes the idea of a universal anticorrelation between these two signals. Furthermore, reaction time, a metric of motor performance, was correlated positively to beta (53%, $r = 0.13$), specifically in the CN, in agreement with previous measurements (*15*), but was only rarely correlated positively or negatively to dopamine release (<17% all CN sites; Fig. 6D).

Thus, motor performance was uniquely correlated to beta and not dopamine activities, showing another dissociation between these two signals and corroborating the idea that they are not generally anticorrelated. Other eye movement parameters including horizontal saccade velocity and amplitudes also were more correlated to the beta signals than to the dopamine signals (table S2). Pupil diameter, also related to autonomic response and arousal, was more highly and positively correlated to the beta signals, and there were mixed positive correlations in the CN (19%) and negative correlations in the putamen (14%; Fig. 6E and table S2). In summary, there were few instances in which dopamine release and beta-band activity were found to be oppositely modulated by behavioral variables, in contradiction to the expected anticorrelation. Moreover, there were cases in which these signals could be modulated in the same direction. Dopamine was correlated negatively with licking at 26% (9 of 34) of session-sites in the putamen, and beta was also correlated negatively at 46% (26 of 56).

These results, together, indicate that dopamine release and beta-band activity were differentially associated with unique aspects of

arousal and autonomic drive, both features of motivation, whereas the beta-band activity provided select associations with motor performance aspects of motivation. Thus, anticorrelated dopamine and beta signaling was not the rule, as these signals often had different and distinct individual correlations to behavioral variables.

We applied univariate multiple linear regression methods to synchronous measures of dopamine release, beta-band activity, and behaviors for the sites that had demonstrated significant negative correlations (table S2) to determine the degree to which the dopamine-beta anticorrelation could be mediated by behavioral variables. A linear model was separately fitted for the dopamine signals or the beta signals using six behavioral parameters (licking, HRV, reaction time, reward size, target saccade direction, and trial number) as predictors. Dopamine levels were then added as a predictor of the beta model and vice versa, and the coefficients and their P values were compared to those for the first two models (table S3). The beta and dopamine striatal signaling parameters were found to be better predictors of each other than were the behavioral variables in both datasets. These results suggest that in the subset of instances in which dopamine and beta displayed anticorrelated activity, this anticorrelation was not mediated by common behavioral inputs related to task parameters or physiological response. This reduced behavioral influence closely ties with the result of a lack of task parameter–selective anticorrelations that had been expected based on the inverse responses of dopamine and beta in discriminating specific reward and movement task variables (Figs. 3 and 5). Thus, an anticorrelated pattern of dopamine and beta signaling does not appear to be a default mode of operation in the brain, specifically in the striatal regions that we explored. Instead, such negatively correlated signals could be uniquely manifested in specific brain sites and states, such as in pathology (e.g., Parkinson's disease), which is an issue that must be explored in future investigations with relevant animal models.

DISCUSSION

These measurements of striatal dopamine levels and beta-band activity are the first to be based on simultaneous recordings in behaving primates. We began with the expectation that the dopamine and beta-band signals would be of opposite polarity. This expectation was based on indirect observations in Parkinson's disease patients: that sustained dopamine depletion and dopamine pharmacological restoration were found to be inversely associated with prolonged (minutes or longer depending on pharmacokinetics and neurodegenerative time course) increases in beta-band signaling during the parkinsonian state and decreases during effective restoration. However, dopamine measurements have not been made in these studies. Therefore, the relative timing and levels of the fast (millisecond) operations of dopaminergic molecular activity and beta-band electrical activity have remained unknown. Our multimodal systems enabled these measurements in task-performing primates, and with these systems, we found that the relationships between dopamine release and beta-band activity were, instead, dynamically regulated across space and task.

First, we found that task-responsive dopamine signals largely followed (by seconds) the earlier ERD beta signals as measured during the same target cue windows, whether of the same polarity or not, and that these early beta-band responses to the cues were phasic relative to the prolonged changes in dopamine release that we measured. Causal manipulations would be needed to interpret the tem-

poral sequencing of these signals, but these different dynamics suggest that the two signaling modes could distinguish different ongoing processing mechanisms.

Second, dopamine release and beta-band activity measured at nearby locations in the striatum were not universally anticorrelated; both negative and positive correlations were identified depending on the relative timing of these signals and task contingencies. The generation of inverse activity was highly contingent on the responsivity of these signals to reward and motor parameters, including prior reward and performance history. These findings suggest that although the rule of anticorrelation holds for trial-averaged responses, a highly nuanced set of controls governs their relative expression patterns when multiple response time frames are considered at the individual trial level.

Third, the dopamine and beta-band signals were differently related to one another at the sites that we sampled in the CN and in the putamen. Their inverse modulation was largely tied to their function in motivated reward evaluation for sites recorded in the CN and to movement parameters for sites recorded in the putamen. Dopamine increases and beta-band decreases were observed for the most part in the context of reward size in the CN and were mostly observed for directional motor function in the putamen. Nevertheless, these apparently spatial preference patterns were not associated with anti- or pro-correlation of the simultaneously recorded dopamine and beta signals. These findings suggest that dopamine and beta-band signals could provide shared roles in reward and motor processing in a regionally dependent manner and that these operations may be largely independent from each other.

At the fine time scales of our measurements, task conditions governed whether the dopamine and beta signals were opposite in polarity, as expected, or were of the same polarity. For example, saccade direction modulated dopamine and beta in the same direction in the CN, and reward size was associated with dopamine and beta changes in the same direction in putamen. As expected, anticipatory licking also had the same polarity of correlation with dopamine and beta in putamen. Dopamine signals related to reward and movement were spatially heterogeneous both within and between the CN and putamen, whereas beta-band activity produced nearly uniform signals in relation to the same behavioral variables. The dopamine signals were influenced by past history, but the beta-band signals were not detectably influenced. This uniformity of the beta-band activity was unlikely to be due to volume conduction, given that the beta signals were always measured using differential signals between pairs of nearby electrodes in the same region. The spatially distinct distribution of dopamine release and beta-band activity that we could resolve emphasizes the likely different and stratified function of these signals in aspects of motor control and value processing and their spatial representations. Higher density multimodal measurements providing greater spatial resolution and distribution of sampling will improve an understanding of the mechanisms underpinning these differences.

Our findings could also be critical to the development of noninvasive beta metrics for clinical applications. These beta metrics have been shown to correlate primarily with motor deficits in Parkinson's disease patients (2, 15) and have been used to improve therapeutic efficacy of closed-loop DBS (5, 6). It is as yet unclear, however, whether they could be used as direct biomarkers of disease mechanism (e.g., dopamine dysregulation) to enable targeting close to the sources of pathology when applied as control signals in closed-loop DBS. We

were able, however, to test directly whether beta-band activity could provide a proxy of concurrent dopamine signaling in the striatum. The beta responses occurred earlier than the dopamine responses, but the patterns of correlation of these signals strongly depended on their relative timing as well as the timing of task events.

These findings indicate that the relationship between dopamine and beta in the non-parkinsonian state is significantly influenced by behavioral contexts and by other parameters outside of these task-relevant parameters. The influences of these multiple factors raise the question of whether, and under what conditions, beta metrics could be practically used as a surrogate for an underlying dopamine dysregulation. Our measurements were made in normal rather than in dopamine-deficient primates, and we focused only on beta-band activity, and not on gamma-band activity, which is thought to act as a pro-movement signal rather than an anti-movement signal as thought for beta-band activity (22). Therefore, the extent to which the current measurements may serve to inform future biomarker-based strategies in the clinic remains unknown. However, the platform that we report here for simultaneous monitoring of dopamine and oscillatory activity, and its flexibility to adapt to new sensor methods, opens a new window to address the ongoing need to achieve an accurate assessment of dopamine dynamics in relation to cell and network function. Our coordinate chemo-electric platform should provide a means in future work to track these signals coordinately over disease progression, helping to identify key neuropathologic features to target in treating Parkinson's disease and other conditions in which dopamine dysfunction occurs.

MATERIALS AND METHODS
Fabrication of implanted sensors
Implanted sensors were silica-based carbon fiber (CF) probes (silica probes) and microinvasive CF probes (μIPs). Silica probes could be manually moved in the brain by turning the screws that lowered the microdrive shuttles to which these were attached. The μIPs were fixed in place and were usually not moved, except during the initial surgical implantation procedure and lowering to target sites in the striatum. The fabrication procedure for the silica probes is detailed in (11). μIPs were fabricated in a similar manner to those created for rodent use (23) but were significantly modified to provide the needed lengths (>10 to 15 mm) to reach the striatal brain structures in primates. Seven-micrometer-diameter CF (Goodfellow, C 005722) was cut into lengths of 20 to 30 mm and then immersed and stored in isopropanol. These were attached to the ends of tungsten rods having lengths of 100 mm and diameters of 75 μm (Goodfellow) using silver epoxy (Epo-tek, H20S). The epoxy was cured on a hot plate (100° to 120°C for 1 to 2 hours). The CF-tungsten assembly was treated for parylene adhesion promotion (23) and then deposited with a conformal layer (0.5 to 2 μm thick) of parylene under vacuum (Specialty Coating Systems, PDS 2010 Labcoater). The CF was exposed by flame-etching the parylene insulated CFs, which extended several millimeters above the water in which the probes were immersed to provide an exposed CF length of ~100 to 300 μm as measured under a microscope. A razor blade was used to trim the exposed CF to a final length of 50 to 200 μm. The final lengths of the parylene encapsulated and exposed CFs extending from the end of the tungsten were 10 to 20 mm. Tungsten shafts were kept outside of the brain during implantation as much as possible. Some of these shafts were threaded through an additional fused silica capillary and

sealed with structural epoxy (Devcon, 14250) if we found that the parylene encapsulation on the shaft had been perforated due to handling. Perforation of the shaft was readily discerned during in vitro electrochemical measurements wherein background current would significantly increase upon immersion of the exposed tungsten areas in saline (0.9%) or artificial cerebrospinal fluid (aCSF) electrolyte. All probes were tested in vitro to ensure background current >300 nA, proportional to exposed CF surface area (10, 20). Background current is related to sensitivity and noise levels (<0.01 nA) and was specified to provide sufficient sensitivity (>20 nA/μM) and limits of detection (1 to 5 nM) of dopamine in vivo, where physiological concentrations are in the nanomolar range in the extrasynaptic space.

Animals and surgeries
Two female rhesus (*Macaca mulatta*) monkeys (subjects M1 and M2, approximately 8.5 and 8 years old, respectively, and both weighing approximately 10 kg, at time of recordings) were used for neural recording and behavioral experiments. All experimental procedures were approved by the Committee on Animal Care of the Massachusetts Institute of Technology. Pole-and-collar methods were used in combination with food or liquid reinforcement to adapt monkeys to transitions from cages to primate chairs. Chronic chambers and grids were installed on both monkeys in two successive surgeries (chamber implantation and craniotomy) performed under sterile conditions and with administration of sevoflurane anesthesia preceded by intramuscular (IM) administration of ketamine (10 mg/kg) and atropine (0.04 mg/kg). Postoperative maintenance included administration of buprenorphine (0.15 to 0.2 mg/kg, subcutaneous), dexamethasone (0.09 to 0.11 mg/kg, IM), ceftriaxone (1.2 to 1.6 mg/kg, IM), and famotidine (0.4 to 0.51 mg/kg, IM). Chambers were placed above the right hemisphere in the coronal plane at angles of 26° and 23° to the sagittal plane for M1 and M2, respectively.

Targeting striatal brain structures with modular chamber platforms
Probes were implanted through form-fitting chambers (obtained from Gray Matter Research) designed to provide access to targeted striatal brain structures in the right hemisphere. Grids installed onto the chambers consisted of an array of holes (24 × 20) with diameters of 0.48 mm and center-to-center distances of 1 mm. Structural 3.0-T magnetic resonance imaging (MRI) (T1-weighted, 0.5 mm isotropic and T2-weighted, 0.35 mm isotropic) was performed for anatomical targeting of implanted probes relative to the grid-hole coordinates. Probes were fixed onto microdrives that allowed screw-controlled movement of probes (158 μm per full turn). In subject M1, 18 probes were chronically implanted into the striatum, of which 8 (2 μIPs and 6 silica probes) were used during the behavioral task performance analyzed in this study. In M2, 19 probes were chronically implanted into the CN and putamen, of which 10 (3 μIPs and 7 silica probes) were used during the behavioral task performance analyzed in this study. All probes exempted from analysis displayed low background current (<300 nA) and/or large amounts of noise (>1 nA) as measured from the FSCV system, and therefore did not meet the minimum operational characteristics. The failure of these probes, despite their operation before implantation, was most likely due to breakage of the CF tip and/or perforation of the insulation during brain insertion. All probes were implanted through a 0.41–mm–outer diameter guide tube (Connecticut Hypodermics, 27G-XTW-'A'-bevel).

The guide tubes penetrated the dura mater and were advanced 5 to 10 mm until they were estimated to be 2 to 5 mm above the boundary of the striatum. Probes were threaded through these guide tubes and were advanced manually or with a micromanipulator (Narishige, MO-97A). Upon reaching initial targeted sites in the striatum, probes were fixed to the microdrives, and the guide tubes were retracted from the brain and retained in the grid holes. In M1, the silica probes were moved every 1 to 4 weeks to sample from multiple sites along a selected insertion track. In M2, all probes were fixed at a target in the striatum and were not moved to maintain the stability of functional measurements over time from a restricted number of implanted sites. In M1, we decided to explore different measurement sites as we had the advantage of an increased number of implantation sites in this subject after ensuring sufficient measurements from the sites that were not repositioned. Site counts reported here are referenced to "sites" for measurements made from the same anatomically distinct sites (i.e., regardless of recording session) and "session-sites" when each site is treated as a different site for different recording sessions. All implanted devices were subjected to low-temperature hydrogen peroxide plasma sterilization (Advanced Sterilization Products, STERRAD).

Synchronous recording of dopamine and electrical neural activity

Dopamine levels were recorded from one to four selected probes using FSCV, and electrical activity was measured from all the remaining probes using standard electrophysiological (Ephys) equipment (see below). We switched the probes assigned to dopamine or LFP recording across recording sessions to be able to acquire both types of signals from each implanted site. FSCV recording probes were connected to a current-to-voltage converter head stage that allowed recording electrochemical current during simultaneous application of a voltage waveform to induce reduction and oxidation (redox) reactions of targeted electroactive chemicals (i.e., dopamine). The head stage was connected to a PC for controlling applied voltage waveforms and for recording and storage of current (system obtained from S. B. Ng-Evans at University of Washington). Ephys recording probes were connected to a voltage-follower head stage (Neuralynx, HS-32) that was connected to an amplification and digitizing system (Neuralynx, Digital Lynx SX). A single ground connection to the animal was provided by the FSCV system and connected to several Ag/AgCl electrodes in the epidural tissue and/or in a white matter region of the brain of the animal. In M1, the ground connection was also tied to the titanium head post and several intracranial titanium screws. The ground connection also served as the FSCV reference. The ground from the Ephys system was connected to the isolation chamber (a box painted with electrically conductive paint in which the monkey performed the task) to provide a Faraday shield around the animal. The concurrent Ephys measurements were only performed in M1.

The FSCV system had a noise level of ~0.1 nA as measured using a "dummy" tissue-emulating load that consisted of a series capacitor of 3.3 nF and resistor of 10 kilohms, with no digital filtering, a dynamic range of ±2000 nA, and a temporal resolution of 175 samples per scan. Each scan consisted of the application of a triangular voltage applied to the probe, changing at a scan rate of 400 V/s to induce electrochemical redox reactions. A scan was made every 100 ms for a sampling frequency of 10 Hz. Background-subtracted pseudo-color plots were created by plotting relative current as color, applied voltage on the y axis (an 8.5-ms voltage scan running from −0.4 V up to +1.3 V and then back down to −0.4 V, applied every 100 ms), and time (i.e., each scan, at 100-ms intervals) on the x axis. Dopamine redox currents are usually identified as current changes at selective potentials, −0.2 and 0.6 V with respect to an Ag/AgCl reference electrode, in the cyclic voltammogram (CV) measured during each scan. Dopamine concentration change is linearly proportional to the oxidation current (i.e., current at the oxidation potential). Current excursions can also occur at other redox potentials that are related to other molecular or ionic species at the sensor. To ensure that the measured current is mostly related to dopamine redox without significant interference, correlation to dopamine standards and principal component regression analyses were performed (see the "Computation of dopamine concentration changes from FSCV-recorded current" section).

The Ephys system was configured to record with an input range of ±1 mV, a sampling rate of 30,000 samples per second, and input filters with a low cut frequency of 0.1 Hz and a high cut frequency of 7500 Hz. The Ephys system also received time stamps of behavioral task events sent from a VCortex behavioral control system (see the "Eye movement task to measure reward bias and movement control" section) using parallel ports to convey 8-bit event codes. A digital messaging system (Neuralynx, NetCom Router) incorporated into the Ephys system and controlled by software functions (MATLAB 2018a) enabled communication of trial-start events from the Ephys system to the FSCV system to provide common time stamps between the two systems. Ephys measurements were made relative to a reference that was connected to several tied epidural stainless steel wires (A-M Systems, 790700). Bipolar derivations were further computed after acquisition as described in the "Beta-band power signal processing" section.

Recording of nonneural physiologic activity

Licking, pupil diameter, pulse, and reaction time were measured to characterize internal behavioral states of the animal during task performance. Licking was measured as the sum of the absolute value of mouthpiece acceleration in all three axes as acquired from the output of a three-axis accelerometer (SparkFun, MMA8452Q) attached to the mouthpiece delivering liquid food to the animal's mouth. These signals were directly routed to the input of the Ephys system after attenuation to scale the signal range down to the range of the recording system (± 5 mV), where they were recorded synchronously with neural electrical activity at the same sample rate. Signals were further processed in software (MATLAB 2018a) to extract relevant features of the raw measurements. The summed three-axis licking signal was then downsampled to 1 kHz and further low-pass–filtered with a cutoff frequency of 100 Hz and smoothed with a Hanning window of 0.1 s or 100 sample width. Pupil diameter was measured from the infrared eye tracking system (SR Research, EyeLink 1000) used for the visually guided task and directly routed into the input of the Ephys system after attenuation. Input filtering was not used in order to retain static (DC) voltage input levels. These signals were also downsampled to 1 kHz. Large variations in the pupil diameter generated during blinking were removed by detecting absolute signal levels above a threshold of 50% of the input range of the recording system (2.5 mV) and interpolating around these points with an additional padding of 30 samples (0.03 s). Normalization was applied to both licking and pupil diameter signals to allow task event–modulated changes to be comparable within and across sessions. Licking was

normalized by taking the standard score (z score) of the measurements across trials for a given session. Pupil diameter was taken as the average signal computed over the 0.2- to 0.8-s window after target cue onset during which the signal was maximally modulated. Averaging windows were matched with windows used for beta metrics for correlations of pupil diameter to beta (table S2). Pupil diameter was normalized by subtracting the average of the pupil diameter for the same trial (from 7 s before to 4 s after the target cue onset, T) and dividing the result by the standard deviation of the pupil diameter in the same trial window. This normalization was done because the range of movements could differ day to day depending on the placement of the mouthpiece relative to the mouth of the animal, and the pupil diameter measurement varied according to environmental lighting and the position of the eye relative to the infrared sensor that could not be accurately reproduced on every session. Pupil diameters were only considered valid for ipsilateral target trials as significant trial-by-trial variations, and drift in the pupil diameter measurements from contralateral target trials was observed. These fluctuations were isolated to contralateral target trials and were most likely caused by ambient light fluctuations due to openings along the door on this side of the isolation chamber for task performance, allowing light transmission from the lab environment to the chamber interior. Pulse was measured from an ear-clipped oximeter (SparkFun, SEN-11574). The signals were routed to the Ephys system in the same way as licking and pupil diameter and downsampled to a final sampling rate of 1 kHz. HRV metrics used in this study were quantified by first identifying peaks in the z score normalized oximeter signal, then finding the interval between peaks, and finally taking the standard deviation of these beat-to-beat interval (RRstd) during defined target-period task event windows (described in the "Signal analysis" section). Reaction time is the measured latency for animals to move their eye to the displayed peripheral target after it was displayed on the screen. Reaction time was derived from the behavioral task system (described in the next section) that controlled the sequence of task events. In Fig. 1D, z score licking (z lick) and pupil diameter (z pupil) traces are aligned to T before averaging (top). Histograms plot the counts of measured reaction time and HRV for each trial over bin widths of 20 and 1 ms, respectively (bottom). Saccade movement parameters including maximum horizontal speed during target acquisition and total integrated horizontal displacement occurring between central fixation cue and target acquisition were computed. Only horizontal components of eye movement were included in these computations as the vertical components were not calibrated (i.e., task performance only required horizontal movements and so only these components were calibrated and used to control the task).

Eye movement task to measure reward bias and movement control

Measurements were made as monkeys performed a visually guided reward-biased task programmed in software (National Institute of Mental Health, National Institutes of Health, VCortex). The monkey was trained to fix on a central cue for 1.6 s, then to make a saccade toward a target that appeared on the left or the right of the screen, and to fixate on the target for 4 s for M1 and 1.8 or 4 s depending on the session for M2 to receive a small reward or big reward. Target eccentricity was 11° to 13°. The left or right spatial positioning of the target relative to the position of the central cue was associated with a small or big reward for a block of 15 to 45 trials in M1 and 50 to 100 trials in M2, after which the association was reversed. The reward was a 50% water-diluted meal shake (Ensure, Plus Nutrition Shake Vanilla) for M2 or a liquid food mixture (355 ml of Plus Nutrition Shake Vanilla, 355 ml of water, blended with two large bananas, and eight biscuits) for M1, delivered through a mouthpiece inside or just outside the monkey's mouth in volumes of 0.1 to 0.3 ml and 1.5 to 2.8 ml for small and large rewards, respectively. The probability of a large reward trial was set to 50% for M1 and 25% for M2. The intertrial interval was set at a fixed value of 7.5 s for M1 and a fixed value between 5 and 15 s fixed for each session for M2. Subjects performed 500 to 1200 trials in each recording session, allowing abundant trial-by-trial and side-by-side comparisons of the neural signals to more accurately define behavioral function and the correlation between dopamine and beta.

Computation of dopamine concentration changes from FSCV-recorded current

All analyses of the neural and behavioral signals were performed using custom software on the basis of standard MATLAB functions (MathWorks, MATLAB 2018a). Dopamine concentration changes ($\Delta[DA]$) were estimated using principal components analysis (PCA) of the FSCV-recorded current, largely as previously described (11). All computations were performed in custom-written software (MATLAB 2018a). Dopamine produces current changes at the reduction and oxidation (redox) potentials of −0.2 and 0.6 V, respectively, with the FSCV parameters applied in this study. To generate a uniform reference signal for all task-modulated signals of interest (e.g., $\Delta[DA]$ during the target cue period), an arbitrary reference time was chosen, usually the alignment event (e.g., target cue). The current recorded at the reference time was then subtracted from the signal of interest to calculate $\Delta[DA]$ relative to the reference. Any signals that produced an excessive variance (Q, or residual sum of squares) above a tolerance level ($Q\alpha$) were removed (the value was set to NaN for analysis purposes at such time points) (11).

Dopamine-associated and non–dopamine-associated currents (i.e., pH and movement artifact) were extracted from the measured background-subtracted electrochemical current by projecting this current onto the principal components computed from standards of dopamine, pH, and movement artifact as previously validated (11). Each subject was provided with a different set of standards due to the different reference electrodes used in each subject, which would shift the redox potentials associated with each chemical component. In M1, 12 dopamine standards, 9 pH standards, and 10 movement standards, and, in M2, 9 dopamine standards, 8 pH standards, and 18 movement standards were created and implemented for PCA. CVs that could not be accounted as a physiological signal were automatically nulled (assigned NaN values) if $Q \geq Q\alpha$. Only dopamine and pH standards were used to calculate the threshold, $Q\alpha$, for each subject. This ensured that current contributions not within expected bounds of primary chemical contributions with a confidence interval of 95% were removed from analysis. $\Delta[DA]$ signals were also nulled at points where CVs were found to be correlated ($r > r_t = 0.8$) to movement standards. The r_t correlation threshold was determined, as previously described (11), to ensure that at least 90% of the signals identified as dopamine were correctly assigned (hit rate), that no more than 30% of known dopamine signals were not identified as dopamine (miss rate), and that no signals were falsely attributed to dopamine (false positives).

Extrapolation of electrical neural activity during synchronous FSCV recording

Spectral interpolation processes were developed and used to remove artifacts in the recorded LFPs induced by the FSCV system (fig. S2). These voltage artifacts arise due to conduction of the currents applied through the FSCV recording probes through the conductive brain tissue around the electrical recording probes. The voltage artifacts observed from the electrical recording probes were periodic (10 Hz) and concomitant with the applied FSCV voltage scans. These 8.5-ms-long artifacts were removed to analyze the naturally occurring LFPs during the hold period (91.5 ms) between the FSCV scans that were made every 100 ms. At least 91.5% of the recorded LFPs were thus preserved intact in every recording. The electrically recorded signals were divided into 5-s windows with a 2.5-s step width and converted to the frequency domain using discrete fast Fourier transform (FFT) functions, where distinct peaks could be detected at the 10-Hz fundamental (applied FSCV frequency) and its harmonics. A piecewise cubic Hermite interpolating polynomial was applied around the fundamental and harmonic peaks at the full width of the individual peaks at 75% of the maximum level with an additional padding equal to the number of samples divided by the sampling frequency (30 kHz) times a factor of 1.25. The interpolated frequency domain signal was then converted back to the time domain using inverse FFT.

We performed these same signal processing steps using artificially constructed data to validate that the interpolation process did not significantly alter the LFP data. The FSCV-generated signals picked up by the electrical recording probes were classified into three types of waveforms based on the observed patterns of the artifacts recorded in the LFPs: monophasic changes (resistive or R type), biphasic changes (resistive-capacitive or RC type), and saturating changes (rail type), where the recorded voltages exceeded the input rails of the head stage amplifier (i.e., signals reached ±1 mV) and also exhibited slow decays most likely related to the saturation recovery rate of the amplifier (rail type). R- and clipping-type artifacts were emulated as charging-discharging RC voltage waveforms that were simply a rising exponential step response of a length equal to the half the FSCV scan duration (4.25 ms) followed by a decaying exponential function of the same length (4.25 ms) function. The time constant was set to 0.75 ms for R-type artifacts to mimic their relatively fast voltage transients and 15 ms for rail-type signals to emulate the longer settling time following saturation of the amplifier. RC-type signals were a superposition of the R-type exponential waveform, with a square wave having the same duration phases. The amplitude of these artifacts was set to equal the standard deviation of the LFP data multiplied by a factor of 6 (average amplitude of the largest FSCV coupled signals observed from recorded signals).

The emulated artifacts were inserted every 100 ms (10-Hz FSCV scan frequency) into clean LFP data that had been recorded without synchronous FSCV (i.e., without FSCV-coupled artifacts). We then compared the original LFP data with the emulated artifact-contaminated LFP data processed with our spectral interpolation methods. This was performed over three different channel recordings of 30-min duration (equivalent to 180 trials each with 10-s duration) and with the three different types of artifacts. The correlation coefficient was computed between the original LFP data and the extrapolated data to ensure that signals coupled be accurately transformed without too much signal alterations. The average correlation coefficient was 0.9884 with a standard deviation of 0.007.

Beta-band power signal processing

Bipolar derivations were created for all Ephys recordings, before spectral interpolation, in an attempt to focalize LFPs to striatal regions overlapping with the FSCV-recorded sites. The recorded activity from a site was subtracted from a nearby site in the same striatal region (CN or putamen) to derive a bipolar pair measurement comprising sites with a range of 1- to 6-mm separation. Each dopamine-recorded site was paired with the bipolar pair comprising the closest electrodes that formed a pair roughly centered on the dopamine recording site to make as fair a comparison between paired dopamine and LFP signals. After spectral interpolation, high-frequency transient spikes and glitches were removed in the signal. This deglitching process was done by identifying these high-frequency transients by taking the differential of the signal and detecting when the signal magnitude exceeded a threshold equal to the absolute value of the mean of the signal times a factor of 7. Linear interpolation was then performed around the peaks of these transients with a width of 1 ms (30 samples). These data were then downsampled by a factor of 30 for a final sample rate of 1 kHz, as the spectrum of apparent task-modulated neural activity was below 100 Hz.

A beta-band frequency range of 13 to 28 Hz was chosen in our studies as it is an established band for defining broad beta-band LFP as reported extensively in work in humans and nonhuman primates (24) and it accommodated the range of task-modulated spectra observed across all our measurement sites within the broadly classified beta spectrum (13 to 35 Hz) (2, 25). Beta spectral content was characterized for all measurement sites in the CN and putamen. LFP spectra were computed with a multitaper approach defined by a time-half-bandwidth product of 3, and five tapers. Spectrograms were created to generate the LFP spectra as a function of time using a 0.75-s window with a 0.15-s step size and averaged over all trials for a fixed condition (e.g., large reward trials) aligned to a specific task event (i.e., target cue onset; fig. S3). The period producing the largest spectral power density in the broadly defined beta range (13 to 35 Hz) was identified for trial averaged spectrogram for each site. The average spectrum during this period was normalized to a fitted pink noise spectrum to help define center and edge frequencies of prominent peak beta amplitude fluctuations in the spectrum outside of the larger amplitudes observed at lower frequency bands largely associated with pink noise. The center frequency (f_c) was identified where the amplitude was maximal in the 13- to 35-Hz band, and the edges (lower and upper frequency limits, f_L and f_H, respectively) were defined by the minima in the spectrum immediately surrounding the center peak. An average f_c of 29 Hz with f_L of 18 and f_H 23 Hz was measured for sites in the CN, and these values were the same whether data were pooled from all session-sites (74 total) or from unique electrode pairs regardless of anatomical repositioning (7 total). An average f_c of 22 Hz with f_L of 16 and f_H 20 Hz was measured for sites in the putamen, and these values were also the same as averaged from all session-sites (63 total) or from unique electrode pairs (12 total).

Beta-band power was computed by first band-pass filtering the LFP data using a Butterworth filter with band-pass frequency limits of 13 and 28 Hz. The same filter was applied first to the reversed data sequence and then again to the reversed output of the first filter, to zero the phase response of the final filtered output. The filtered data were squared, and then an envelope was fitted to the peaks of the squared data. The enveloped data were then smoothed with a Hanning window of 0.25-s (250-sample) full-width. This window was chosen to provide meaningful comparisons of beta power and

dopamine fluctuations during the same task windows, where the corresponding dopamine signals did not show significant fluctuations faster than this chosen window size. Last, the smoothed data were downsampled to the FSCV sampling frequency of 10 Hz.

Signal analysis

Signals were aligned to target-cue onset for all successfully completed trials in each session. Baseline subtraction of the computed dopamine signals (described in the "Computation of dopamine concentration changes from FSCV-recorded current" section) was applied by subtracting the signal at the target-cue onset for each trial measurement to provide a uniform reference frame for task-selective dopamine changes over the short target-RW time scale. This is done to remove background drift associated with FSCV-based measurements that can create significant fluctuations in the recorded current (*11*, *21*). Typically, this electrochemical current is stable for a period of 15 to 60 s, which is longer than any individual trial (<6 s), and signals containing significant drift are automatically excluded as detected by the residual variances exceeding tolerance thresholds ($Q \geq Q\alpha$, as described in the "Computation of dopamine concentration changes from FSCV-recorded current" section). Trials were removed from analysis based on the following exclusion criteria: (i) more than 30% of the computed dopamine concentration changes within the trial (defined as the period between central cue onset and reward delivery) consisted of movement-related artifacts (these signals were previously assigned to nonnumeric, i.e., NaN, values, such that they did not contribute to the analysis) or CVs not ascribable to dopamine, pH, or background drift, or (ii) any of the beta was above 20 times the trial mean or if the beta signal during the entire trial was above 20 times the mean of all trials within a session.

Signals aligned to the target cue were averaged across trials within an individual session and an individual site for different task conditions (big versus small reward, contralateral versus ipsilateral target, and task history). These averaged time-varying waveforms allowed distinguishing of the patterns of neural and behavioral signal dynamics between different task conditions.

Trial-by-trial analysis was performed to extract distinct time variable features of the signals for each individual trial. Several metrics were explored to identify signal characteristics during the target period (period between target cue and reward delivery) that showed a significant discrimination between task conditions (big versus small reward, contralateral versus ipsilateral target, and task history). For all metrics, the target-period window was padded with a 0.2-s offset applied after the initial window boundary (i.e., target cue) and before the last window boundary (i.e., reward delivery) to remove signals related to neighboring events as most of the signals were found to change significantly 0.1 to 0.3 s following the target cue onset. For the "peak" metric, for which dopamine signals showed the greatest discrimination between task conditions, the maximum value of the signals within the entire target period was used for each trial. For the "window" metric, all signals were averaged within the entire target period (0.2 to 3.8 s) for each trial to obtain a response value for each trial. For sessions in which shorter target periods were used (i.e., M2 had a target fixation period of 1.8 s), the peak metric was computed in the same manner, but the averaging window for the window metric was calculated from 0.2 s after T to 0.2 s before the reward outcome (i.e., 1.6 s for a 1.8-s target period). We computed the beta-power signal averaged over the 1-s window (0.2 to 0.8 s) immediately following the target cue onset, as this early beta metric best discriminated the

same reward and movement direction task variables as the dopamine peaks. Choice of the time windows used to average and compute these task-modulated beta signals is further described in the subsequent section ("Metrics of task-modulated beta").

These trial-by-trial signal response values were aggregated for the different task conditions for a given site in a given session to evaluate differences in signal responses between task conditions. The values grouped for task condition were normalized to assess relative differences between conditions and to compare measurements across sites and sessions as shown in the scatter plots in Figs. 2 to 4. Significance ($P < 0.05$) of the difference between groups of neural responses between conditions was determined by the *t* test. Grouped values were generated only if there were more than five valid trials for each group used in comparison. Dopamine values were normalized by dividing all values for a given site and session by the absolute value of the median of all values. Beta values were normalized by subtracting the mean of all values and dividing this by the difference of the maximum and minimum beta values for a given site pair and session.

Each beta value plotted in the figures or reported in the main text, unless otherwise noted, represents the bipolar signal from the pair of LFP recording sites associated with an individual dopamine-recorded site (as explained in the "Beta-band power signal processing" section). All of the beta measurements irrespective of the dopamine-recorded sites are shown in fig. S6.

Correlational analyses

Significant anticorrelations were observed at 17 of 25 site-specific pairs (number of sites displaying a significant correlation in at least one recording session), at 24 of 56 paired session-sites (i.e., paired sites counted independently over different sessions), at 33 of 171 all session-sites (i.e., all possible region-matched paired dopamine and beta correlations irrespective of proximity, 1 to 6 mm, between sites, used to calculate 19% figure reported in the main text), and in 17 of 20 recorded sessions. The correlations were calculated on pairs of dopamine and beta-signal responses measured in the same trials for a given session and site. The Bonferroni correction was applied for the two comparisons of dopamine peak versus beta early window and dopamine peak versus beta whole window. We then identified recorded sites and sessions demonstrating significant correlations with a corrected $mP < 0.05$, where $m = 2$ is the number of comparisons. Significant anticorrelations were chosen for the window that provided the lowest P value. The average correlation coefficient of significant anticorrelations observed between distinct site pairs was −0.128. Correlations were also explored for other beta averaging windows, not used in the statistical figures reported in the main text, and these are shown in table S2. Correlations were also calculated between other types of signals (e.g., dopamine versus lick and beta versus lick). HRV trial responses were calculated as the RRstd computed during 1- to 4-s window immediately following target cue in each trial. Licking responses were calculated as the average licking activity during the 0- to 2-s window following the target cue in each trial. Reaction time was computed for each trial as the time from the target cue onset to the onset of a saccade to this target. Results of comparisons showing a significant number of site counts statistically different from zero ($P < 0.05$, binomial test) are reported in the main text and are indicated in red in table S2. Correlations between dopamine and beta were calculated in specific task conditions to evaluate whether the inverse (Figs. 3B and 5C) and common (Figs. 3C and 5B) polarity responses were mediated by direct correlation of the dopamine

and beta. A binomial test was used to compare the expected number of correlated sites based on the significant number of responsive sites (shown in Figs. 3, B and C, and 5, B and C) and to compare this to the actual number of correlated sites.

Metrics of task-modulated beta

Several metrics were explored to define beta signals modulated by task parameters and in correlation to the dopamine peaks and non-neural physiological response signals. Cue-evoked beta-band power modulation is commonly computed by averaging the beta-band power over a discrete time window that is several hundreds of milliseconds or seconds wide following a task-relevant stimulus (25). A similar averaging window, "early" beta defined as the window 0.2 to 0.8 s after cue, was applied in our measurements to define task-modulated beta. We further extended our analysis over the entire task period to explore periods over which beta and concomitant dopamine recordings might covary outside of more narrowly defined early beta period. The covariance between the dopamine and beta signals recorded within each trial was computed as a function of time relative to target onset for each pair of simultaneously recorded, spatially adjacent recordings (see the "Beta-band power signal processing" section) (Fig. 2B). All such measurements then were averaged for all trials in every session. This procedure allowed identification of time periods in which beta-band power showed a trend of correlating predominantly positively or predominantly negatively with dopamine. These averaged covariance data demonstrated a peak correlation magnitude (correlation coefficient of −0.04) at 0.7-s posttarget cue for the beta signal.

We determined the influence of the beta power averaging window on our results by systematically exploring an array of time periods with various starting and ending times during the target period. We used the window that maximized the number of sites showing differences between task conditions to characterize task-modulated beta signals. These differences were computed by averaging the beta over the chosen time window for each trial and then performing a t test for a difference between conditions for each site. This window was sometimes found to be different for CN and putamen. We found an early period of 0.2 to 0.8 s for discriminating reward size in CN and putamen, as well as movement direction in CN. Another period of 0.2 to 3.8 s (window) was found to discriminate movement direction in the putamen. Significant correlations of beta to dopamine peaks and physiological response varied largely depending on the chosen beta averaging windows. Correlation matrices between dopamine and beta are shown in Fig. 2D for all possible site pairs. Significant correlations are tabulated for the early and the window periods, as well as the window in which the maximum number of correlations was observed: 0.2 to 3.2 s in CN and 0.2 to 2.6 s in putamen (table S2). Only the early period and the window in which maximal correlation was observed are shown for correlation results tabulated between beta and physiological response (table S2). The latency of the ERD, another metric for beta signal modulation (15), was also explored by calculating the time point in which beta-band power was minimal over the 1-s period following the target cue onset. Only 5 of 171 sites showed significant positive correlations, and 5 of 171 sites showed significant negative correlations to dopamine peaks.

Signals related to large and small reward

Both dopamine and beta data were available from monkey M1. In the CN, dopamine peaks were greater for large RW targets than for small RW targets when these targets appeared in the contralateral hemifield ($P < 0.05$ at 15 of 24 sites in M1, t test; Fig. 2C, top), whereas RW size had no effect for targets in the ipsilateral hemifield (fig. S4A, left). Similarly, the decrease in early beta signals was greater for the large RW targets than for small RW targets, but there was no dependence on which hemifield the target appeared in ($P < 0.05$ at 12 of 24 sites for contralateral targets and 20 of 24 sites for ipsilateral targets in M1, t test; fig. S4B, left).

However, in the putamen, dopamine peaks were unexpectedly smaller for large RW targets than for small RW targets in the contralateral hemifield ($P < 0.05$ at 10/34 sites, where all 10 sites were reward sensitive, constituting 10 of 12 reward-sensitive sites, in M1, t test; Fig. 2D, top). Reward size induced mixed responses in the dopamine peaks for ipsiversive targets (fig. S4A, right). Early beta signals again maintained larger decreases for large RW than for small RW regardless of laterality ($P < 0.05$ at 14 of 34 sites for contralateral and 25 of 34 sites for ipsilateral in M1, t test; fig. S4B, right).

Only dopamine data were available from monkey M2. In the CN, dopamine peaks were greater for large RW targets than for small RW targets when ipsilateral and contralateral target trials were grouped ($P < 0.05$ at 3 of 11 sites in M2, t test; fig. S4E, left), but the difference was not significant when ipsilateral and contralateral trials were analyzed separately (fig. S4C, left). In the putamen, dopamine peaks were greater for large RW targets than for small RW targets in the contralateral hemifield ($P < 0.05$ at 2/7 sites in M2, t test; fig. S4E, right), unlike M1. Nevertheless, dopamine peaks were smaller for large RW targets than for small RW in the ipsilateral hemifield ($P < 0.05$ at 2/7 sites in M2, t test) and big RW preferring dopamine increases observed for contralateral targets (fig. S4C, right). The dopamine peaks were greater for large RW targets than for small RW when ipsilateral and contralateral target trial conditions were grouped together ($P < 0.05$ at 2 of 17 sites in M2, t test; fig. S4E).

Signals related to task history

Reward and performance history also had an effect on dopamine responses, but not on beta-band signals. Dopamine measured on a given trial was significantly different depending on whether the previous trial's outcome was a large or small RW and whether the monkey had successfully performed or had failed to make the appropriate eye movements to obtain RW in the previous trial. These task history–dependent dopamine changes were observed at 11 of 23 CN or 12 of 34 putamen sites as related to RW history, and 11 of 23 CN or 12 of 34 putamen sites as related to performance history, in M1 ($P < 0.05$, t test; Fig. 3). RW and performance history both showed the same effect on dopamine responses measured at one site in the CN of M2, but only RW history generated a significant difference as measured in the aggregate of all seven recorded sites in the putamen of M2 ($P < 0.05$, t test). Task history had little effect on the beta signals measured in M1. Four of 46 sites in the CN and 1 of 68 sites in the putamen showed the expected inverse (greater suppression) following negative RW or performance experiences ($P < 0.05$, t test; Fig. 3C and figs. S4 and S5).

Signals related to movement control

Dopamine and beta signals were highly dependent on movement direction in an RW-contingent manner. Dopamine peaks were greater in the putamen of M1 when saccades were made to contralateral targets than to ipsilateral targets during small RW trials ($P < 0.05$ at 9 of 10 movement-responsive sites or 9 of 34 all sites, in M1, t test; Fig. 4B,

top), and mixed responses were observed related to movement direction for large RW trials (fig. S4F, right). Dopamine peaks were greater in the CN of M1 for ipsiversive saccades than for contraversive saccades in small RW trials ($P < 0.05$ at 10 of 24 sites, in M1, t test; Fig. 4F, left). Beta decreases were greater for contraversive movements than for ipsiversive movements, displaying the inverse response to putaminal dopamine, at 7 of 34 sites in the putamen and at 15 of 24 sites in the CN, for small RW trials (Fig. 4G).

In the putamen of M2, dopamine peaks were smaller when saccades were made to contralateral targets than to ipsilateral targets at one of seven sites during small RW trials ($P < 0.05$, t test) and greater for contralateral targets than for ipsilateral targets at two of seven sites during large RW trials ($P < 0.05$, t test; fig. S4H).

Other physiological response correlations

Correlations of dopamine and beta to physiological response and motor performance metrics including licking, pupil diameter (for ipsilateral trials only, as explained in the "Recording of nonneural physiologic activity" section), saccade velocity and amplitude (for horizontal eye movement components only, as explained in the "Recording of nonneural physiologic activity" section), and HRV are counted and tabulated for all dopamine- and beta-recorded sites in table S2. Methods for characterizing these correlations are discussed in the "Signal analysis" section. Representative examples of correlated signals are shown in Fig. 6. Licking correlated positively with dopamine at 67% of all CN session-sites ($r = 0.15$, average of significant positive correlations, $P < 0.05$) and correlated negatively with beta at 48% of all CN session-sites ($r = -0.15$, average of negative correlations, $P < 0.05$). Pupil diameter correlated positively with early beta at 23% of all session-sites ($r = 0.16$, average of significant positive correlations, $P < 0.05$). Saccade velocity correlated positively with beta (as averaged over the window of 2 to 3.8 s that displayed maximal correlations), especially in contralateral target trials at 25% of all CN session-sites ($r = 0.18$, average of positive correlations, $P < 0.05$). Saccade amplitude correlated positively with beta (early window), especially in ipsilateral target trials at 37% of all CN session-sites ($r = 0.19$, average of positive correlations, $P < 0.05$). HRV correlated positively with dopamine in 21% of all CN session-sites ($r = 0.09$, average of positive correlations, $P < 0.05$) and correlated negatively with beta (as averaged over the window of 0.2 to 2 s that displayed maximal correlations) especially in small reward trials at 20% of all CN session-sites ($r = -0.19$, average of negative correlations, $P < 0.05$). Reaction time was significantly correlated to beta in the CN ($r = 0.13$, average of significant correlations, $P < 0.05$, 14 of 19 of all session-site pairs in CN or 15 of 19 sessions or 8 of 15 of all site pairs in CN) and significantly less to dopamine (positive correlations at 3 of 19 and negative correlations at 1 of 19 of all session-site pairs in CN or less than 2 of 12 of all CN sites; Fig. 6D).

Multiple linear regression modeling

Univariate multiple linear regressions were performed using the "fitlm" function in MATLAB. Data were included from each of the 33 pairs of dopamine and beta recordings that showed statistically significant anticorrelations in the CN during the 0.2- to 3.2-s window or in the putamen during the 0.2- to 2.6-s window. Each dopamine or beta recording and each behavioral parameter were separately normalized (z scored) for each recording session. CN recordings and putamen recordings were then separately aggregated across sites and sessions to fit the linear models.

Four univariate multiple linear regressions were performed on each of two datasets: dopamine and beta values averaged over the 0.2- to 3.2-s time window displaying maximum negative dopamine-beta correlations for the CN sites (table S2) and over the 0.2- to 2.6-s window for putamen. A linear model was separately fitted, in the first two linear regressions, for the dopamine signal or the beta signal using six behavioral parameters (anticipatory licking, HRV, reaction time, reward size, saccade direction, and trial number) as predictors. Dopamine level was then added as a predictor to the beta model and vice versa, and the coefficients and their P values were compared to those for the first two models (table S3). The neural parameters (beta and dopamine) were better predictors of each other than were the behavioral variables in both datasets.

Trial number was the most heavily weighted and most statistically significant predictor in the first two models, followed by reward size, for both dopamine and beta in the CN. Dopamine became the strongest and most significant predictor of beta, and the significant coefficients all decreased slightly in magnitude when dopamine was added as a predictor to the beta model. Beta was a strong and highly significant predictor of dopamine, although it was eclipsed by trial number and reward size in coefficient magnitude when beta was added as a predictor to the dopamine model. The significant coefficients again diminished slightly in magnitude when beta was added, except for reaction time, whose coefficient slightly increased.

There were fewer significant behavioral parameters in the putamen than in the CN. Trial number was once again a strong predictor of dopamine levels, but saccade direction was slightly stronger. The strongest predictor of beta levels in the putamen was HRV, followed closely by reaction time. Trial number was weak and not even close to being statistically significant. When we added dopamine as a predictor to the beta model, it was by far the strongest and most significant predictor, and the coefficient for HRV decreased in magnitude. Adding beta to the dopamine model similarly showed beta to be a much better predictor than behavioral parameters and caused the other coefficients' magnitudes to diminish slightly.

REFERENCES AND NOTES

1. P. Damier, E. C. Hirsch, Y. Agid, A. M. Graybiel, The substantia nigra of the human brain: II. Patterns of loss of dopamine-containing neurons in Parkinson's disease. *Brain* **122**, 1437–1448 (1999).
2. N. Jenkinson, P. Brown, New insights into the relationship between dopamine, beta oscillations and motor function. *Trends Neurosci.* **34**, 611–618 (2011).
3. T. Kononowicz, H. van Rijn, Tonic and phasic dopamine fluctuations as reflected in beta-power predict interval timing behavior. *Proc. Soc. Behav. Sci.* **126**, 47 (2014).
4. P. V. Agostino, R.-K. Cheng, Contributions of dopaminergic signaling to timing accuracy and precision. *Curr. Opin. Behav. Sci.* **8**, 153–160 (2016).
5. G. Tinkhauser, A. Pogosyan, S. Little, M. Beudel, D. M. Herz, H. Tan, P. Brown, The modulatory effect of adaptive deep brain stimulation on beta bursts in Parkinson's disease. *Brain* **140**, 1053–1067 (2017).
6. S. Little, M. Beudel, L. Zrinzo, T. Foltynie, P. Limousin, M. Hariz, S. Neal, B. Cheeran, H. Cagnan, J. Gratwicke, T. Z. Aziz, A. Pogosyan, P. Brown, Bilateral adaptive deep brain stimulation is effective in Parkinson's disease. *J. Neurol. Neurosurg. Psychiatry* **87**, 717–721 (2016).
7. N. Mallet, A. Pogosyan, A. Sharott, J. Csicsvari, J. P. Bolam, P. Brown, P. J. Magill, Disrupted dopamine transmission and the emergence of exaggerated beta oscillations in subthalamic nucleus and cerebral cortex. *J. Neurosci.* **28**, 4795–4806 (2008).
8. A. Devergnas, D. Pittard, D. Bliwise, T. Wichmann, Relationship between oscillatory activity in the cortico-basal ganglia network and parkinsonism in MPTP-treated monkeys. *Neurobiol. Dis.* **68**, 156–166 (2014).

9. M. Weinberger, N. Mahant, W. D. Hutchison, A. M. Lozano, E. Moro, M. Hodaie, A. E. Lang, J. O. Dostrovsky, Beta oscillatory activity in the subthalamic nucleus and its relation to dopaminergic response in Parkinson's disease. *J. Neurophysiol.* **96**, 3248–3256 (2006).

10. M. M. McCarthy, C. Moore-Kochlacs, X. Gu, E. S. Boyden, X. Han, N. Kopell, Striatal origin of the pathologic beta oscillations in Parkinson's disease. *Proc. Natl. Acad. Sci. U.S.A.* **108**, 11620–11625 (2011).

11. H. N. Schwerdt, H. Shimazu, K.-i. Amemori, S. Amemori, P. L. Tierney, D. J. Gibson, S. Hong, T. Yoshida, R. Langer, M. J. Cima, A. M. Graybiel, Long-term dopamine neurochemical monitoring in primates. *Proc. Natl. Acad. Sci. U.S.A.* **114**, 13260–13265 (2017).

12. R. Kawagoe, Y. Takikawa, O. Hikosaka, Reward-predicting activity of dopamine and caudate neurons—A possible mechanism of motivational control of saccadic eye movement. *J. Neurophysiol.* **91**, 1013–1024 (2004).

13. M. W. Howe, P. L. Tierney, S. G. Sandberg, P. E. M. Phillips, A. M. Graybiel, Prolonged dopamine signalling in striatum signals proximity and value of distant rewards. *Nature* **500**, 575–579 (2013).

14. P. N. Tobler, C. D. Fiorillo, W. Schultz, Adaptive coding of reward value by dopamine neurons. *Science* **307**, 1642–1645 (2005).

15. A. A. Kühn, D. Williams, A. Kupsch, P. Limousin, M. Hariz, G.-H. Schneider, K. Yarrow, P. Brown, Event-related beta desynchronization in human subthalamic nucleus correlates with motor performance. *Brain* **127**, 735–746 (2004).

16. H. B. Parthasarathy, J. D. Schall, A. M. Graybiel, Distributed but convergent ordering of corticostriatal projections: Analysis of the frontal eye field and the supplementary eye field in the macaque monkey. *J. Neurosci.* **12**, 4468–4488 (1992).

17. N. Eshel, J. Tian, M. Bukwich, N. Uchida, Dopamine neurons share common response function for reward prediction error. *Nat. Neurosci.* **19**, 479–486 (2016).

18. Y. Hori, T. Minamimoto, M. Kimura, Neuronal encoding of reward value and direction of actions in the primate putamen. *J. Neurophysiol.* **102**, 3530–3543 (2009).

19. M. Matsumoto, O. Hikosaka, Two types of dopamine neuron distinctly convey positive and negative motivational signals. *Nature* **459**, 837–841 (2009).

20. H. M. Bayer, P. W. Glimcher, Midbrain dopamine neurons encode a quantitative reward prediction error signal. *Neuron* **47**, 129–141 (2005).

21. A. A. Hamid, J. R. Pettibone, O. S. Mabrouk, V. L. Hetrick, R. Schmidt, C. M. Vander Weele, R. T. Kennedy, B. J. Aragona, J. D. Berke, Mesolimbic dopamine signals the value of work. *Nat. Neurosci.* **19**, 117–126 (2015).

22. M. Cassidy, P. Mazzone, A. Oliviero, A. Insola, P. Tonali, V. Di Lazzaro, P. Brown, Movement-related changes in synchronization in the human basal ganglia. *Brain* **125**, 1235–1246 (2002).

23. H. N. Schwerdt, E. Zhang, M. J. Kim, T. Yoshida, L. Stanwicks, S. Amemori, H. E. Dagdeviren, R. Langer, M. J. Cima, A. M. Graybiel, Cellular-scale probes enable stable chronic subsecond monitoring of dopamine neurochemicals in a rodent model. *Commun. Biol.* **1**, 144 (2018).

24. K.-i. Amemori, S. Amemori, D. J. Gibson, A. M. Graybiel, Striatal microstimulation induces persistent and repetitive negative decision-making predicted by striatal beta-band oscillation. *Neuron* **99**, 829–841.e6 (2018).

25. A. A. Kühn, L. Doyle, A. Pogosyan, K. Yarrow, A. Kupsch, G.-H. Schneider, M. I. Hariz, T. Trottenberg, P. Brown, Modulation of beta oscillations in the subthalamic area during motor imagery in Parkinson's disease. *Brain* **129**, 695–706 (2006).

Citation: H. N. Schwerdt, K. Amemori, D. J. Gibson, L. L. Stanwicks, T. Yoshida, N. P. Bichot, S. Amemori, R. Desimone, R. Langer, M. J. Cima, A. M. Graybiel, Dopamine and beta-band oscillations differentially link to striatal value and motor control. *Sci. Adv.* **6**, eabb9226 (2020).